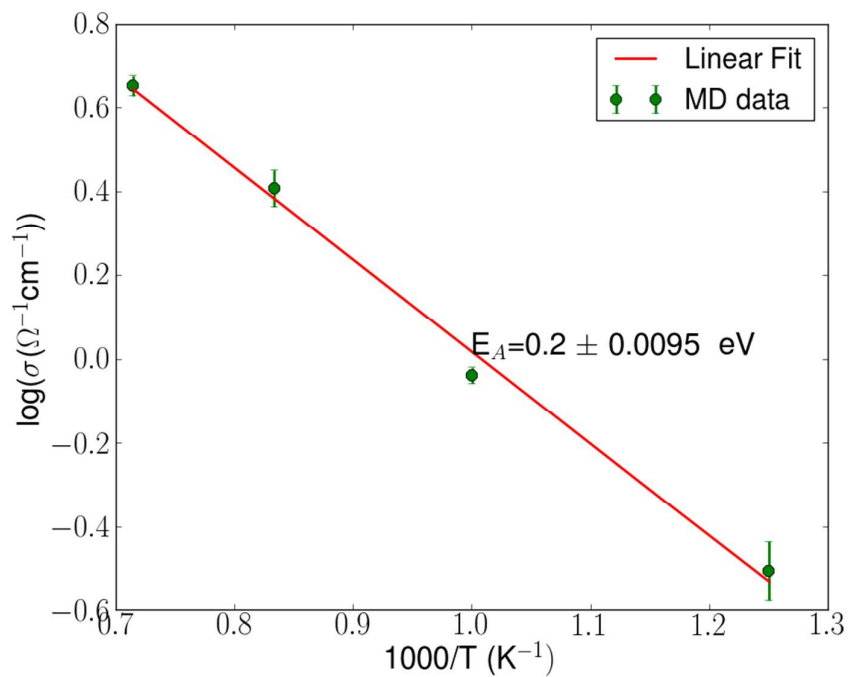


**Theoretical prediction of a highly conducting solid electrolyte for sodium battery: Na₁₀GeP₂S₁₂**

Journal:	<i>Journal of Materials Chemistry A</i>
Manuscript ID:	TA-ART-03-2015-001616.R1
Article Type:	Paper
Date Submitted by the Author:	08-May-2015
Complete List of Authors:	Kandagal, Vinay; Center for Study of Science Technology and Policy, Bharadwaj, Mridula; Center for Study of Science, Technology and Policy, Waghmare, Umesh V; Jawaharlal Nehru Centre for Advanced Scientific Research, Theoretical Sciences Unit

Graphical Abstract



The theoretically predicted compound $\text{Na}_{10}\text{GeP}_2\text{S}_{12}$ exhibits Na-ionic conductivity of the same order of magnitude as that of other state-of-the-art solid electrolytes used in practical sodium batteries such as high-temperature sodium–sulfur battery.

ARTICLE

Theoretical prediction of a highly conducting solid electrolyte for sodium battery: Na₁₀GeP₂S₁₂

Cite this: DOI: 10.1039/x0xx00000x

Vinay S. Kandagal^{*a}, Mridula Dixit Bharadwaj^a and Umesh V. Waghmare^b

Received 00th January 2012,

Accepted 00th January 2012

DOI: 10.1039/x0xx00000x

www.rsc.org/

Using first-principles simulations, we predict a high-performance solid electrolyte with composition Na₁₀GeP₂S₁₂ for use in sodium-sulfur (Na-S) batteries. Thermodynamic stability of its structure is established through determination of decomposition reaction energies and phonons, while Na-ionic conductivity is obtained using ab initio molecular dynamics at elevated temperatures. Our estimate of the room-temperature (RT) conductivity is 4.7 x 10⁻³ Scm⁻¹, which is slightly higher than those of other superionic solid electrolytes such as β''-alumina and Na₃Zr₂Si₂PO₁₂, currently used in practical high-temperature Na-S batteries. Activation energy obtained from the Arrhenius plot (in the range 800-1400 K) is 0.2 eV, which is slightly lower than the typical values exhibited by other ceramic conductors (0.25-1 V) (Hueso et al., *Energy Environ Sci.*, 2013, 6, 734). We show that soft Na-S phonon modes are responsible for its thermodynamic stability and the lower activation barrier for diffusion of Na-ion. Finally, the calculated electronic bandgap of 2.7 eV (a wide electrochemical window) augurs well for its safe use in sodium batteries. Opening up a possibility of realizing RT operation of Na-S batteries, our prediction of a new phase in the Na-Ge-P-S system will stimulate experimental studies of the material.

I. Introduction

Energy efficient, safe batteries are crucial in integrating renewable energy to the existing power-grid. Sodium-sulfur (Na-S) batteries have been widely deployed around the world for stationary applications (34 MW Na-S installation to support 51 MW wind farm in Japan is the largest battery based storage system in the world¹). In this system, Na and S react during discharge to form polysulfide compounds with compositions ranging from Na₂S₅ to Na₂S₃. To prevent their precipitation (and hence cell failure) as well as to achieve high Na⁺ conductivity through the β''-alumina electrolyte, the battery is operated at temperatures as high as 300-350°C². This poses safety concerns and requires the use of expensive containers and sealants². An effective approach in improving its safety as well as reducing operational costs would be to enable room-temperature (RT) operation of such a battery without considerable reduction in energy and power density. Several efforts are already being made in this direction³⁻⁶.

Important challenges in designing RT Na-S battery include a) achieving high ionic conductivity through the electrolyte at room temperature, and b) suppressing the loss in capacity due to polysulfide shuttling⁷. In the shuttling effect, the polysulfide products formed during a discharge dissolve in the liquid organic electrolytes and get transferred from cathode to anode through the separator. This results in reduction of the amount of effective material involved in energy storage. *Solid* electrolytes can be explored as a potential solution for overcoming this problem. The ceramic β''-alumina is a state-of-the-art sodium solid electrolyte with ambient temperature conductivity of 2 mScm⁻¹ (Ref. ⁸). Wenzel et al.⁹ used it in combination with a liquid electrolyte in their RT Na-S battery, and found the capacity losses reduced in comparison to the use of liquid-only electrolytes. A sulfide based electrolyte, glass-ceramic Na₃PS₄, has recently enabled all-solid-state RT Na-S battery, and was shown to interface well with electrodes³. Similar such compounds are being explored further⁵. Solid electrolytes offer additional advantages over liquids such as increased safety, and enable lighter and more compact batteries. There is need for development of novel compositions/chemistries of solid Na-ion conductors. Specifically, design of a solid electrolyte with conductivity in the range 10⁻³-10⁻² Scm⁻¹ will contribute considerably towards realizing practical all-solid-state RT Na-S batteries.

^aCenter for Study of Science Technology and Policy, 10th cross Mayura street, Papanna Layout, Nagashettihalli, Bengaluru, Karnataka 560094, India. Email: vinayk@cstep.in

^bJawaharlal Nehru Centre for Advanced Scientific Research, Jakkur, Bengaluru, Karnataka 560064, India.

Kamaya et al.¹⁰ recently reported a solid electrolyte with composition $\text{Li}_{10}\text{GeP}_2\text{S}_{12}$ (LGPS) for application in lithium batteries which showed an extremely high Li^+ conduction of $12 \times 10^{-3} \text{ Scm}^{-1}$ at room temperature and a high stability window of 5 V. The material consists of framework made up of LiS_6 octahedra, LiS_4 , PS_4 , and $(\text{Ge}_{0.5}\text{P}_{0.5})\text{S}_4$ tetrahedra. While Li-ions were proposed to diffuse along the 1D channels along c direction, first-principles simulation studies later showed possible diffusion pathways in ab plane as well¹¹. It is evident that sodium can form compounds similar to lithium; for example, solid electrolyte compounds such as $x\text{Li}_2\text{S}+(1-x)\text{P}_2\text{S}_5$ and $x\text{Na}_2\text{S}+(1-x)\text{P}_2\text{S}_5$, $\text{Li}_2\text{S-GeS}_2$ and $\text{Na}_2\text{S-GeS}_2$ exist¹²⁻¹⁴. Therefore a sodium compound analogous to LGPS with composition $\text{Na}_{10}\text{GeP}_2\text{S}_{12}$ (NGPS) can be envisaged (Hueso et al.⁸ have also proposed the idea in their review article). In the current study we employ first-principles calculations to predict the structure, stability and the Na^+ conductivity of a novel composition - $\text{Na}_{10}\text{GeP}_2\text{S}_{12}$ (NGPS). Our predictions will stimulate experimentalists on the fabrication and further improvement of this material. While Na-P-S compounds exist, and are being investigated for potential electrolytes lately^{3,5}, a single phase of Na-Ge-P-S system has not been reported so far. Hence the current study, for the first time, also presents a possibility of a new phase in the Na-Ge-P-S system.

Mo et al.¹¹ and Ong et al.¹⁵ have carried out density functional theory (DFT) calculations of the structure, electrochemical window and Li^+ diffusivities of LGPS. The experimentally reported structure has partial occupancies in Li and Ge/P sites. Ong et al.¹⁵ reduced the set of possible structures (resulting due to partial occupancies) using electrostatic energy as the criterion. Among these structures, the one with the lowest DFT energy was used in their modelling studies. They found that minimization of electrostatic energy led to a structure with tetragonal $\text{P4}_2/\text{mc}$ space group (same as experimentally reported) while the structure with the lowest DFT energy had a slightly distorted tetragonal form with P1 space group. The DFT energies of the two structures differed slightly (~ 10 meV/atom). Using this structure, Ong et al.¹⁵ have carried out further investigation on the effect of cationic and anionic substitution in LGPS on Li^+ conductivity. We benefit here from the knowledge on LGPS and related structures obtained from experiment as well as first-principles calculations, and explore the possibility of Na-analogue of LGPS for a high performance solid electrolyte.

II. Methodology

The structure and sodium ion diffusivities in NGPS are determined using quantum density functional theory (DFT) calculations with Projector augmented wave (PAW)^{16,17} method and Perdew-Burke-Ernzerhof (PBE)^{18,19} exchange correlation functional as implemented in the Vienna Ab initio Simulation Package²⁰⁻²³ (VASP) program. As mentioned earlier, we use the unit cell structure of LGPS with the lowest DFT energy as predicted by Ong et al.¹⁵, and substitute sodium atoms in place of lithium. The structure is then fully relaxed through energy minimization and used in subsequent analysis. Our work is divided into three major components:

- 1) *Phase stability analysis*: Total energy, phonons and decomposition reaction energies determined within DFT calculation are used to evaluate the phase stability. We

identified seven possible reactions by which NGPS can decompose into various compounds of Na, P, Ge and S as listed (except Na_4GeS_4) in the Inorganic Crystal Structure Database²⁴. Ground-state energies of these reactions are determined to assess the stability of the predicted material against decomposition.

- 2) *Bandgap*: Electrochemical window is determined to assess the voltage range in which the electrolyte can operate.
- 3) *Ionic conductivity*: Ab initio molecular dynamics simulations are performed at four different temperatures ranging from 800 to 1400 K in the NVT ensemble. Radial distribution functions and Na-ion diffusivities are evaluated. We benchmarked numerical parameters of our simulations through comparison with published results for LGPS by Mo et al.¹¹ The system (NGPS) is heated from an initial temperature of 100 K to 800 K in 2.8 ps, and later evolved for 50 ps. The rate of heating used in the present work is 250 K/ps - approximately half of that used by Mo et al.¹¹ for simulating LGPS, with a time-step of 2 fs. To reduce the computational cost, a lower energy cutoff of 300 eV is used instead of 600 eV—the cut-off at which the ground-state structure converged. It is seen that a structural distortion resulting from displacing an atom by 0.04 Å in each of the three axes directions results in similar change in total energy calculated with energy cutoff of 300 and 600 eV, and hence forms the basis for choosing the lower cutoff. A uniform mesh of $2 \times 2 \times 2$ k-points is used for sampling the Brillouin zone.

Following equations are used in subsequent analysis. Vibrational contribution to free energy is obtained as:

$$S_{\text{vib}} = -k_B \int g(\omega_i) \log \left[2 \sinh \left(\frac{\hbar \omega_i}{2k_B T} \right) \right] d\omega \quad (1)$$

Where S_{vib} is the vibrational entropy, $g(\omega_i)$ is the density of states of phonon with frequency ω_i . T is the temperature, k_B is the Boltzmann constant and \hbar is the Planck's constant. The diffusivity coefficients and corresponding conductivities at different temperatures are calculated as:

$$D = \frac{1}{2d} \frac{\langle (r(t+t_0))^2 - (r(t_0))^2 \rangle}{t} \quad (2a)$$

where $t_0 = 0, \Delta t, 2\Delta t, 3\Delta t, \dots$ and $t = \Delta t, 2\Delta t, 3\Delta t, \dots$

$$\sigma = \frac{C_i z_i^2 F^2 D}{RT} \quad (2b)$$

$$\sigma = \sigma_0 \exp \left(-\frac{E_A}{RT} \right) \quad (2c)$$

Where C_i is the Na-ion concentration in the compound, Z_i is the magnitude of charge on Na ion, F is the Faraday's constant; R is the gas constant, T is temperature, D is diffusivity coefficient, d is dimensionality (equal to 3 in this case), σ is the conductivity, E_A is the activation energy and Δt denotes a timestep in MD simulation.

III. Results and Discussion

1. Phase Stability

Starting with the structure of the unit cell of LGPS as an initial guess, structural optimization resulted in a slightly distorted tetragonal crystal structure of NGPS (see Figure 1) with unit cell parameters $a=9.327$ Å, $b=9.841$ Å, and $c=13.903$ Å, and angles $\alpha=90.681$, $\beta=91.270$, and $\gamma=90.068$. We now present analysis of the stability of this phase using the unit cell of NGPS consisting two formula units (fifty atoms) in a periodic box with dimensions equal to unit cell parameters.

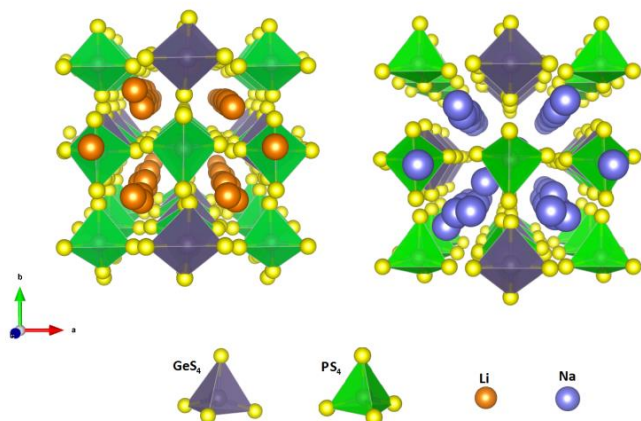


Fig. 1 Comparison of structures (unit cells) of $\text{Li}_{10}\text{GeP}_2\text{S}_{12}$ (as predicted by Ong et al.¹⁵) and the predicted $\text{Na}_{10}\text{GeP}_2\text{S}_{12}$ compound. Both structures exhibit the same tetrahedral framework consisting GeS_4 and PS_4 .

a) Phonons

Phonons are essentially the quantized vibrational normal modes of a material, and their frequencies (ω) reflect the stiffness of bonds in the material. Phonon frequencies are obtained as square root of the eigenvalues of the Hessian (matrix of second derivatives of energy w.r.t atomic displacements weighed by inverse masses). An imaginary frequency (negative second derivative of energy) precisely indicates a structural instability. If $\omega^2 > 0$ for all frequencies, the structure is at an energy minimum and hence locally stable. Thus, the phonon spectrum is effective in assessing on the stability of the material. Figure 2 compares the distribution of Γ -point phonon states as a function of frequency for both NGPS and LGPS wherein negative frequencies are used to indicate the imaginary values. The plots are obtained by introducing a gaussian function of suitable width centered on each frequency to yield a smooth curve. Since all the ω 's of the predicted NGPS material span positive frequencies, we establish that the material is structurally at least metastable or locally stable. Furthermore, higher density of states at lower frequencies in NGPS than in LGPS suggests that it is relatively more stable than its Li counterpart, particularly at elevated temperatures.

Following observations can be made from the inspection of the eigenvectors of phonons. Higher energy modes ($500\text{-}570$ cm^{-1}) in both the materials are mainly from the vibrations involving P and S atoms of PS_4 tetrahedra. In LGPS, modes less than 450 cm^{-1} arise mainly from the Li-S bonds followed by Ge-S bonds. In NGPS,

three distinct bands are seen. Major contributions from Na-S bonds are mainly observed in the first band (upto 300 cm^{-1}), and the middle band ($330\text{-}405$ cm^{-1}) has contribution primarily from Ge-S bonds of the GeS_4 tetrahedra. An important finding is that NGPS has relatively more number of states at lower frequencies than in LGPS that involve Na-S bonds, and are expected to enhance Na^+ ion diffusivity.

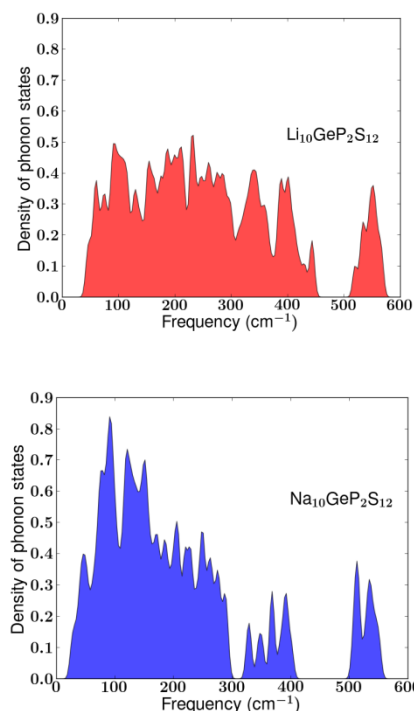


Fig. 2 Density of states of Γ -point phonons as a function of frequencies for the LGPS (top) and NGPS (bottom).

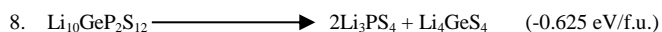
Table 1 Possible decomposition reactions of NGPS and the corresponding calculated energies (expressed per formula unit of NGPS)

SL. No.	Possible decomposition Reactions of NGPS	Energy (eV/f.u.)
1.	$\text{Na}_{10}\text{GeP}_2\text{S}_{12} \longrightarrow 2\text{Na}_3\text{P} + \text{GeS}_2 + 2\text{Na}_2\text{S}_5$	11.8
2.	$\text{Na}_{10}\text{GeP}_2\text{S}_{12} \longrightarrow 2\text{Na}_3\text{PS}_4 + \text{GeS}_2 + 2\text{Na}_2\text{S}$	0.72
3.	$2\text{Na}_{10}\text{GeP}_2\text{S}_{12} \longrightarrow 5\text{Na}_2\text{S} + \text{GeS}_2 + \text{P}_2\text{S}_5$	2.2
4.	$4\text{Na}_{10}\text{GeP}_2\text{S}_{12} \longrightarrow 8\text{Na}_3\text{PS}_4 + \text{Na}_4\text{Ge}_4\text{S}_{10} + 6\text{Na}_2\text{S}$	0.61
5.	$2\text{Na}_{10}\text{GeP}_2\text{S}_{12} \longrightarrow 4\text{Na}_3\text{PS}_4 + \text{Na}_6\text{Ge}_2\text{S}_7 + \text{Na}_2\text{S}$	-0.07
6.	$\text{Na}_{10}\text{GeP}_2\text{S}_{12} \longrightarrow 2\text{Na}_3\text{PS}_4 + \text{Na}_2\text{GeS}_3 + \text{Na}_2\text{S}$	-0.11
7.	$\text{Na}_{10}\text{GeP}_2\text{S}_{12} \longrightarrow 2\text{Na}_3\text{PS}_4 + \text{Na}_4\text{GeS}_4$	-0.147

b) Reactions of decomposition of NGPS: energetics

To establish chemical stability of NGPS, we considered the chemical reactions shown in Table 1 (above), representing different ways in

which the proposed structure may decompose, and estimated corresponding energies expressed per formula unit of the reactant. The negative energies in the final three reactions in the table mean that they are exothermic and may occur spontaneously, indicating the reactant's instability. Mo et al.¹¹ similarly proposed the following reaction which favours the decomposition of LGPS:



Reaction 7 (in Table 1) is analogous to this reaction for LGPS, but has a smaller energy gain. The compound Na_4GeS_4 has not been reported in the literature or the ICSD, and was obtained by DFT optimization of the structure analogous to that of Li_4GeS_4 , obtained by replacing Li with Na. The Li_4GeS_4 structure was obtained from The Materials Project²⁵.

Stability of LGPS against reaction 8 was attributed to entropic effects at higher temperatures (including room temperature)¹¹. The total entropy change ΔS for the compound was evaluated approximately by Du et al.²⁶, and is given by the sum $\Delta S_{\text{config_Li}} + \Delta S_{\text{mix_P/Ge}} + \Delta S_{\text{vib}}$. The first term represents configurational entropy due to partial occupancies of Li sites, and the second term is the mixing entropy due to P and Ge disorder in the originally reported structure¹⁰. These two terms can be assumed to be the same for NGPS also due to similarity in the structures of both compounds. We evaluated vibrational entropy ΔS_{vib} as a function of temperature for both compounds using equation (1) with the Γ -point phonon states, and find that NGPS has slightly higher vibrational entropy (Figure 3), as expected from its softer phonons ($\omega < 100 \text{ cm}^{-1}$). We can therefore, safely say the total entropies $\Delta S_{\text{NGPS}} > \Delta S_{\text{LGPS}}$, which means that the entropic effects are slightly stronger in the sodium compound. Since the energy gain in reaction 7 (for NGPS) is weaker than that of reaction 8 (for LGPS), and the fact that LGPS is stable at room temperature, we expect NGPS to be stabilized by entropic effects at ambient and higher temperatures.

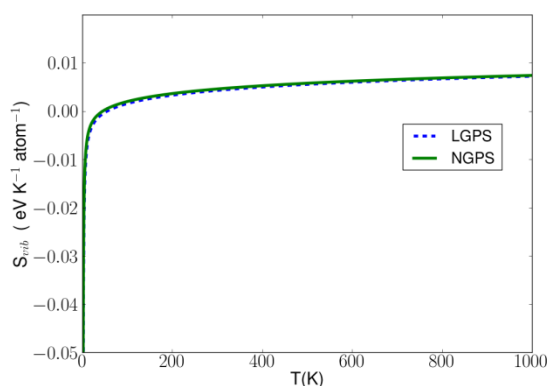


Fig. 3 Vibrational entropy calculated according to equation (1), of the two electrolytes, LGPS and NGPS.

1. Electrochemical window (E_g)

The HSE06 hybrid functional²⁷ has been widely used for electrochemical window (E_g) calculations. Using this functional, Mo et al.¹¹ reported a value of 3.6 V for LGPS

which is much lower than the experimentally determined value of 5 V¹⁰. This discrepancy was attributed to a possible passivation phenomenon at the electrode interfaces leading to the formation of compounds such as Li_2S at the anode and P_2S_5 at the cathode, but these reactions have not been observed so far in experiments^{10,28}. An alternate explanation proposed²⁶ recently is that the addition/removal of Li^+ in LGPS, keeping the structural framework intact possibly results in its higher observed electrochemical window. However, the reason for its wider observed electrochemical window is still unclear.

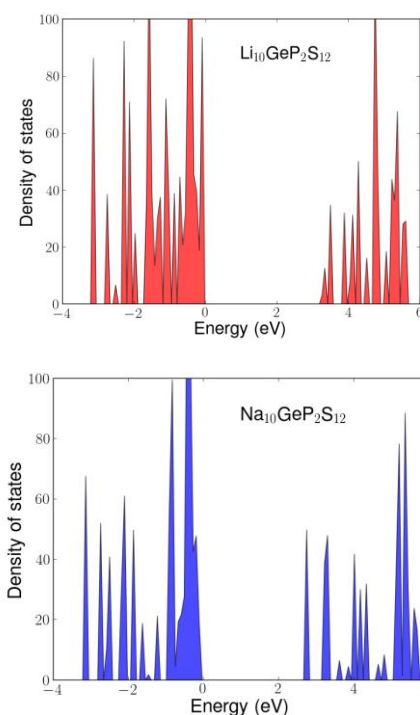


Fig 4: Electronic density of states for both LGPS (top) and NGPS (bottom). The figures show the bandgap for LGPS to be 3.2 as opposed to experimentally determined value of over 5 V, and for NGPS the calculated value is 2.7 V.

Using the HSE06 hybrid functional, our estimate of E_g of NGPS is 2.7 V, and for LGPS it is 3.2 V (Figure 4). Our value for LGPS is 0.4 V less than Mo et al.'s calculations. This may be due to accounting of additional vacant orbitals in the pseudopotentials used in their calculations. Nevertheless, we find that the calculated potential window for NGPS (2.7 V) falls in the range of voltages exhibited by many sodium ion cathodes and the sodium sulphur batteries (1.78-2.08 V)⁶. However, we note the considerable discrepancy between DFT calculated and experimentally determined values of the bandgap for LGPS, and conclude that one may have to resort to experiments for a more reliable estimate for the structurally similar sodium compound.

2. Ab initio Molecular dynamics

We have used ab initio MD to evaluate two main properties: the radial distribution functions and Na^+ diffusivities. During these

simulations the total energy at all temperatures fluctuated around a constant average which further confirms the stability of the proposed NGPS structure. Fluctuations in energy per atom varied in the range 0.4-1% of the mean energy per atom at all the temperatures considered.

a) Radial distribution functions (g(r))

We examined the radial distribution functions (g(r)) obtained from MD simulations which provide structural information of the material in terms of inter-atomic distances and coordination numbers. Figure 5 shows partial g(r) of LGPS and NGPS, calculated from the MD trajectories at 800 K. The first and second peaks in both figures occur at 2 and 2.3 Å corresponding to P-S and Ge-S bonds respectively. This means that the cationic species Na or Li does not affect these bonds. Due to larger size of Na atom, Na-X (X=Ge, P, S) distances are longer than corresponding Li-X distances as expected. As mentioned previously, no single phase involving Na-P-Ge-S is reported in the literature for comparison of the predicted interatomic distances. However, a comparison of Na-X distances can be made with other sulfide based sodium ion conductors available in the literature. Table 2 shows such a comparison with Na₂S-GeS₂, which has also been studied for electrolyte applications. Itoh and Fukunaga²⁹ investigated the structure of Na₂S-GeS₂ glass using experimental (shown in Table 2) and reverse Monte Carlo simulation methods. In this material, the Ge-S and Na-S bonds are of two types: with and without common bridging sulphur. The distances compared in Table 2 involve non-bridging sulphur (similar to NGPS).

Tetragonal Na₃PS₄ electrolyte studied by Jansen and Henseler³⁰ is structurally similar to NGPS, but exhibits lower conductivity (of the order of 10⁻³ mScm⁻¹ at 50 °C). It consists of PS₄ tetrahedral framework whereas NGPS structure consists of PS₄ and (Ge_{0.5}P_{0.5})S₄; formed by alternately replacing PS₄ by GeS₄ tetrahedra. Hence it is reasonable to compare the bond distances in the two compounds, and we find that the sodium environments in the two materials are quite similar. It can be seen from Table 2 that the predicted interatomic distances in NGPS are comparable to the corresponding values seen in other similar compounds.

b) Sodium ionic diffusion coefficients and conductivities

Diffusion coefficients and ionic conductivities are calculated using the equations (2a) and (2b) at four different temperatures: 800, 1000, 1200 and 1400 K. Such high temperatures are considered to achieve quicker convergence, and hence shorten the simulation time (they are seen to converge over the time period of 50 ps). The room-temperature Na-ion diffusivity/conductivity is then obtained by extrapolation from these four points via the Arrhenius plot (shown in Figure 6a). The Na-ion diffusion coefficients calculated at higher temperatures are compared to those of Li in LGPS in Figure 7. It is evident that sodium ion diffusivities are higher than lithium at temperatures above 1200 K.

Arrhenius plot of conductivity versus temperature as shown in the Figure 6a, fits quite well (with a goodness of fit (R²) equal to 99.6%) to a linear curve. From the plot, the extrapolated conductivity at room temperature (300 K) is 4.7 mScm⁻¹. This is of the same order of magnitude as exhibited by polycrystalline β''- alumina. The

activation energy obtained as the slope of the linear plot in Figure 6a is 0.2 ± 0.0095 eV, a bit lower than that of Li-ion diffusion in LGPS (0.24 eV) calculated from results at similar temperatures¹¹. The activation energy (for NGPS) is lower than the typical values exhibited by other ceramic ionic conductors (refer Table 3), which range from 0.25 to 1 eV⁸.

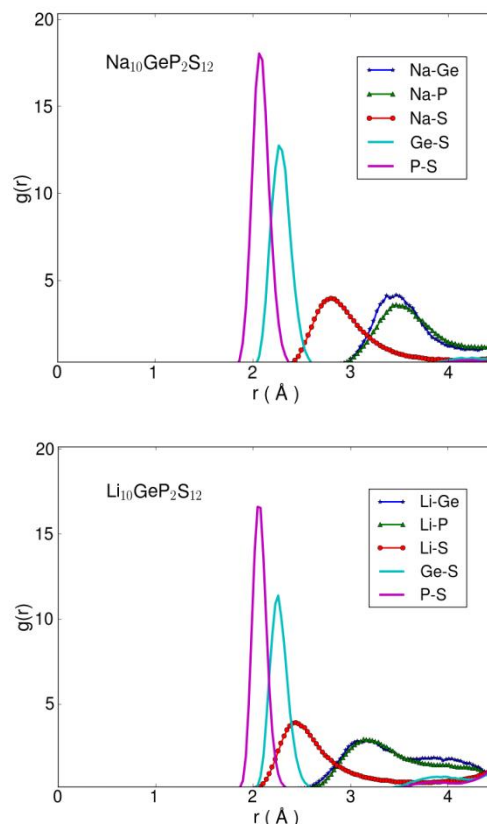


Fig. 5: Partial radial distribution function of LGPS (top) and NGPS (bottom), calculated from MD simulation at 800 K.

Table 2 Comparison of the predicted interatomic distances in NGPS with corresponding values found experimentally in two other solid electrolytes. The distances in NGPS correspond to first peaks in the partial g(r) calculated at 800 K (shown in Figure 5). (NA in the table refers to the unavailability of the corresponding experimental value).

	Na ₁₀ GeP ₂ S ₁₂ (at 800 K)	(Na ₂ S) ₅₀ ·(GeS ₂) ₅₀ (glass) (Ref. 29)	Na ₃ PS ₄ (tetragonal) (Ref. 30)
Na-S	2.78	2.8	2.9-3.01
Na-Na	3.6	3.1	3.5
Na-Ge	3.45	NA	-
Na-P	3.48	-	3.5
Ge-S	2.27	2.23	-
P-S	2.07	-	2.04

LGPS was shown to exhibit a higher Li diffusivity in the c direction compared to that in the ab plane. Whereas in case of NGPS, similar trend is observed upto a certain temperature (~ 1300 K), beyond which diffusion in ab plane is seen to be higher than that along the c axis. Furthermore, for both the cases of diffusion considered (axial and planar), Na in NGPS exhibits lower activation energies (0.127 ± 0.022 and 0.251 ± 0.019 eV) than those for Li (0.17 and 0.28 eV) in LGPS as calculated by Mo et al.¹¹ It can be seen from Figure 6b that diffusion of Na^+ is expected to occur predominantly along the c direction at lower temperature.

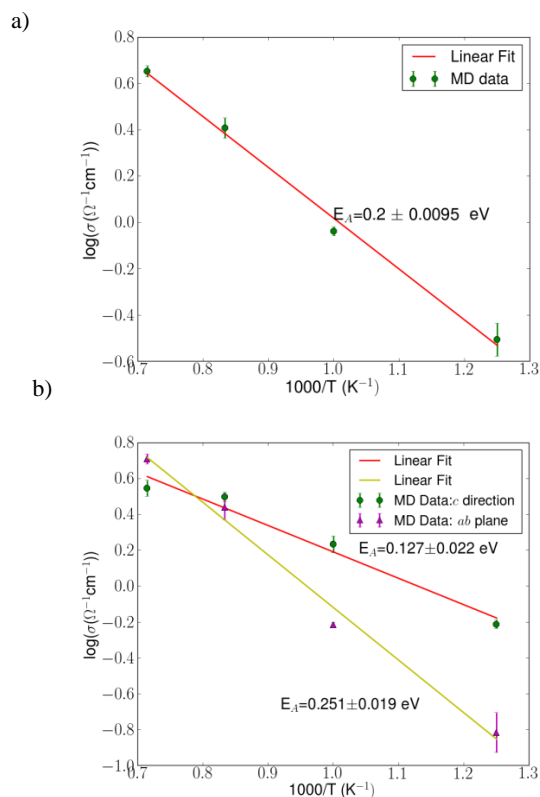


Fig. 6: Arrhenius plot of Na^+ conductivities at four different temperatures. a) Total conductivity, b) Conductivity along c direction and in ab plane. Corresponding activation energy values are also shown.

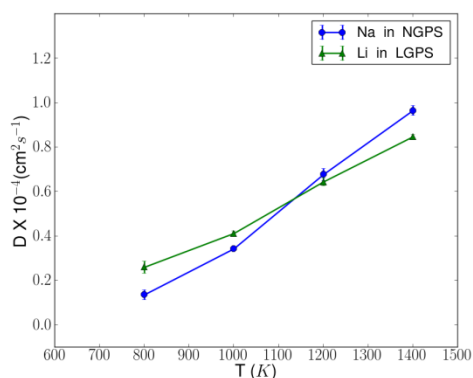


Fig. 7: Diffusivity coefficients of Na in NGPS and Li in LGPS at different temperatures.

We now compare the ionic conductivity with different high- Na^+ ion conducting solid electrolytes at room temperature and their corresponding activation energies (see Table 4). β -alumina solid electrolyte (BASE) and NASICON are the two widely used solid electrolytes in high temperature sodium batteries. The conductivities of both the electrolytes depend on the methods of their preparation. BASE exists in two different crystal structures⁸ - β -alumina (with composition $\text{Na}_2\text{O} \cdot (8-11)\text{Al}_2\text{O}_3$) and β'' -alumina ($\text{Na}_2\text{O} \cdot (5-7)\text{Al}_2\text{O}_3$). The latter exhibits higher Na^+ ion conductivity (single crystal β'' -alumina can exhibit conductivity of the order of $40-100$ mScm^{-1} , see Ref.31).

Table 4: Comparison of room temperature conductivities of NGPS with other sodium electrolytes currently being used/studied. NASICON stands for sodium super ionic conductor.

Name of the sodium conductor	Conductivity mScm^{-1}			Activation energy (eV)	Ref.
	25 °C	50 °C	300 °C		
Single crystal β'' - alumina	40			0.22 (25 – 200 °C) 0.17 (250-650 °C)	33
			1000	0.33 (25 – 150 °C) 0.10 (> 150 °C)	33
Poly. β'' - alumina	2		220 – 350	0.15 – 0.26	8
			360	0.18 (285-330 °C)	33
$\text{Na}_{1+x}\text{Zr}_2\text{Si}_x\text{P}_{3-x}\text{O}_{12}$ ($0 < x < 3$) NASICON	3.4		100 – 200	0.32 – 0.38 (< 157 °C) 0.13 – 0.24 (> 157 °C)	31
			182.68	0.2 (527–1127 °C)	34
$\text{Na}_{10}\text{GeP}_2\text{S}_{12}$ (predicted)	4.7		135.6	0.2 ± 0.0095 (> 527 °C)	present work
$94\text{Na}_3\text{PS}_4 \cdot 6\text{NaSiS}_4$	0.74			0.28	32
Na_3PS_4 (glass ceramic)	0.2			0.416	3
$\alpha\text{-Na}_3\text{PS}_4$		0.0042		0.54	30
50 Na_2S – 50 GeS_2		$\sim 10^{-4}$			3

Commercial β'' - alumina manufactured by Ionotec Ltd exhibits a room temperature conductivity of 2 mScm^{-1} (Ref.⁸). At 573 K, which is the operating temperature of Na-S battery, its conductivity is 240 mScm^{-1} (Ref.⁸). NASICON stands for sodium superionic conductor, and has a generic composition $\text{Na}_{1+x}\text{Zr}_2\text{Si}_x\text{P}_{3-x}\text{O}_{12}$ ($0 < x < 3$). Na^+ conductivity of NASICON produced by Ceramtec, Inc. (USA) is $3-4$ mScm^{-1} at room temperature³¹. The calculated ionic conductivity in NGPS in the current study is higher than that of both

polycrystalline β'' -alumina and NASICON at room temperature, but lower at the operating temperature of Na-S or sodium metal chloride battery.

Sulfides of sodium are an important class of glass/glass-ceramic electrolytes. Their conductivities are however lower than BASE and NASICON materials. Hayashi et al.³ demonstrated room-temperature operation of an all-solid-state Na-S battery with a novel glass-ceramic electrolyte containing cubic Na_3PS_4 , which showed a Na^+ conductivity of 0.2 mScm^{-1} . This is of the same order of magnitude as that predicted here of NGPS. A major advantage of the mentioned sulphide electrolyte is that it formed a good interface with electrodes upon simple cold pressing. Another sulphide based solid electrolyte which enabled such a RT-Na/S battery, but with enhanced capacity, was reported by Nagata et al.⁵ Tanibata et al.³² reported a room temperature Na^+ ion conductivity of 0.74 mScm^{-1} for $94\text{Na}_3\text{PS}_4\text{-}6\text{Na}_4\text{Si}_3\text{S}_4$, which is the highest value reported so far for sulfides. Compared to both the above mentioned electrolyte and cubic Na_3PS_4 , NGPS is expected to exhibit a better performance in terms of Na-ionic conductivity. However, one should note that solid electrolytes can exhibit different activation energies in different temperature ranges (as seen for BASE and NASICON in Table 4). Hence the activation energy for NGPS may be different (slightly higher) at lower temperatures than the one calculated here, thereby resulting in lower room-temperature conductivity.

Conclusions

Benefiting from the knowledge established in solid electrolytes of Li-batteries and using first-principles simulations, we have established a thermodynamically stable structure of NGPS, which exhibits a high Na^+ conductivity and wide electrochemical window that make it a promising candidate for efficient and safe use in RT-Na-S batteries. The study also presents for the first time the possibility of a single phase in the Na-Ge-P-S system.

Phase stability of the new compound ($\text{Na}_{10}\text{GeP}_2\text{S}_{12}$) is established from its free energy and comparison with the analogous phase of Li ($\text{Li}_{10}\text{GeP}_2\text{S}_{12}$). Based on the consideration of decomposition energies and entropies, it is noted that NGPS is more stable than LGPS, and also has an electrochemical window of 2.7 V which is favourable for Na-S battery operation.

Sodium ionic conductivity is calculated at elevated temperatures (800 – 1400 K) from *ab initio* MD calculations, and extrapolated to obtain the same at lower temperatures. The ambient temperature conductivity is found to be higher than that in commercially used polycrystalline β'' -alumina and NASICON electrolytes, though it is relatively lower at 573 K (operating temperature of Na-S battery). Soft vibrational modes of Na-S bonds evident in the phonon spectrum are responsible for high diffusivity of Na^+ ions as well as the material's thermodynamic stability.

Preparation techniques of currently used electrolytes such as BASE and $\text{Na}_3\text{Zr}_2\text{Si}_2\text{PO}_{12}$ are involved and energy intensive. They may further need chemical modification to enhance other desirable

properties such as mechanical strength. Our results should stimulate experimental studies to synthesize $\text{Na}_{10}\text{GeP}_2\text{S}_{12}$ for electrolyte applications and explore how it is advantageous over existing electrolytes in aspects such as cost, ease of preparation, mechanical stability and safety.

Acknowledgements

This paper is based upon work supported under the US-India Partnership to Advance Clean Energy-Research (PACE-R) for the Solar Energy Research Institute for India and the United States (SERIUS), funded jointly by the U.S. Department of Energy (Office of Science, Office of Basic Energy Sciences, and Energy Efficiency and Renewable Energy, Solar Energy Technology Program, under Subcontract DE-AC36-08GO28308 to the National Renewable Energy Laboratory, Golden, Colorado) and the Government of India, through the Department of Science and Technology under Subcontract IUSSTF/JCERDC-SERIUS/2012 dated 22nd Nov. 2012. VSK and MDB would also like to thank Tanmay Sarkar, Arghya Bhowmik and Dr Parveen Kumar for useful suggestions in carrying out the simulations.

References

- 1 Z. Wen, Y. Hu, X. Wu, J. Han and Z. Gu, *Adv. Funct. Mater.*, 2013, **23**, 1005–1018.
- 2 C. Daniel, J. O. Besenhard and Wiley InterScience (Online service), *Handbook of battery materials*, Wiley-VCH Verlag, Weinheim, 2011.
- 3 A. Hayashi, K. Noi, A. Sakuda and M. Tatsumisago, *Nat. Commun.*, 2012, **3**, 856.
- 4 S. Zheng, P. Han, Z. Han, P. Li, H. Zhang and J. Yang, *Adv. Energy Mater.*, 2014, **4**, n/a–n/a.
- 5 H. Nagata and Y. Chikusa, *Chem. Lett.*, 2014, **43**, 1333–1334.
- 6 S. Xin, Y.-X. Yin, Y.-G. Guo and L.-J. Wan, *Adv. Mater.*, 2014, **26**, 1261–1265.
- 7 I. Bauer, M. Kohl, H. Althues and S. Kaskel, *Chem. Commun.*, 2014, **50**, 3208.
- 8 K. B. Hueso, M. Armand and T. Rojo, *Energy Environ. Sci.*, 2013, **6**, 734.
- 9 S. Wenzel, H. Metelmann, C. Reiß, A. K. Dürr, J. Janek and P. Adelhelm, *J. Power Sources*, 2013, **243**, 758–765.
- 10 N. Kamaya, K. Homma, Y. Yamakawa, M. Hirayama, R. Kanno, M. Yonemura, T. Kamiyama, Y. Kato, S. Hama, K. Kawamoto and A. Mitsui, *Nat. Mater.*, 2011, **10**, 682–686.
- 11 Y. Mo, S. P. Ong and G. Ceder, *Chem. Mater.*, 2012, **24**, 15–17.
- 12 S. S. Barbano, I. Seo, C. M. Bischoff, K. E. Schuller and S. W. Martin, *J. Non-Cryst. Solids*, 2012, **358**, 93–98.
- 13 R. K. Sista and M. Seshasayee, *J. Non-Cryst. Solids*, 2004, **349**, 54–59.
- 14 M. Ribes, B. Barrau and J. Souquet, *J. Non-Cryst. Solids*, 1980, **38-39**, 271–276.
- 15 S. P. Ong, Y. Mo, W. D. Richards, L. Miara, H. S. Lee and G. Ceder, *Energy Environ. Sci.*, 2013, **6**, 148.
- 16 P. E. Blöchl, *Phys. Rev. B*, 1994, **50**, 17953–17979.
- 17 G. Kresse, *Phys. Rev. B*, 1999, **59**, 1758–1775.
- 18 J. P. Perdew, K. Burke and M. Ernzerhof, *Phys. Rev. Lett.*, 1996, **77**, 3865–3868.
- 19 J. P. Perdew, K. Burke and M. Ernzerhof, *Phys. Rev. Lett.*, 1997, **78**, 1396–1396.

ARTICLE

- 20 G. Kresse and J. Hafner, *Phys. Rev. B*, 1993, **47**, 558–561.
- 21 G. Kresse and J. Hafner, *Phys. Rev. B*, 1994, **49**, 14251–14269.
- 22 G. Kresse and J. Furthmüller, *Comput. Mater. Sci.*, 1996, **6**, 15–50.
- 23 G. Kresse, *Phys. Rev. B*, 1996, **54**, 11169–11186.
- 24 G. Bergerhoff, R. Hundt, R. Sievers and I. D. Brown, *J. Chem. Inf. Model.*, 1983, **23**, 66–69.
- 25 A. Jain, S. P. Ong, G. Hautier, W. Chen, W. D. Richards, S. Dacek, S. Cholia, D. Gunter, D. Skinner, G. Ceder and K. A. Persson, *APL Mater.*, 2013, **1**, 011002.
- 26 F. Du, X. Ren, J. Yang, J. Liu and W. Zhang, *J. Phys. Chem. C*, 2014, **118**, 10590–10595.
- 27 J. Heyd, G. E. Scuseria and M. Ernzerhof, *J. Chem. Phys.*, 2003, **118**, 8207.
- 28 A. Kuhn, V. Duppel and B. V. Lotsch, *Energy Environ. Sci.*, 2013, **6**, 3548.
- 29 K. Itoh and T. Fukunaga, *Solid State Ion.*, 2009, **180**, 351–355.
- 30 M. Jansen and U. Henseler, *J. Solid State Chem.*, 1992, **99**, 110–119.
- 31 Coors W. G., Gordon J. H., and Menzer S. G., *US Patent* US2010/0297537A1(2010).
- 32 N. Tanibata, K. Noi, A. Hayashi and M. Tatsumisago, *RSC Adv.*, 2014, **4**, 17120.
- 33 Z. Yang, J. Zhang, M. C. W., Meyer-Kintner, X. Lu, D. Choi, J. P. Lemmon and J. Liu, *Chem. Rev.*, 2011, **111**, 3577–3613.
- 34 P. Colomban, *Solid State Ion.*, 1986, **21**, 97–115.